Advances in Natural Science **ISSN 1715-7862 [PRINT]**
Vol. **3**, No. **2**, **2010**, pp. 17-26 **ISSN 1715-7870 [ONLINE]**
www.cscanada.net **www.cscanada.org**

The 3rd International Conference of Bionic Engineering

Simulation Study of Bionic Jetting Direction Influence on Drag Reduction Effect

ZHAO Gang[1]
ZHAO Hua-lin[2]
SHU Hai-sheng[3]
ZHAO Dan[4]
GU Yun-qing[5]
XIA Dong-lai[6]

Abstract：By imitating the jetting flow feature of shark gills，a bionic jetting model is established by arranging round outlets on a flat plate. The drag reduction effect under different jetting directions are explored using numerical simulation method when the main flow field velocity was 20m/s and the reasons of drag reduction are analyzed simultaneously. The results of simulation showed that：different jetting directions affect the wall shear stress and static pressure of flow field which result in the changing of viscous resistance and pressure drag; the bionic jetting has the best drag reduction effect when jetting direction angle is 30 degrees; under different jetting direction conditions, the main reason of drag reduction is the substantially decreased pressure drag.
Key words: bionics; drag reduction; jetting flow; numerical simulation; viscous resistance; pressure drag

1. INTRODUCTION

Researches on drag reduction technologies have been received significant attentions in the past decades. Many engineering applications in aeronautics, marine and pipelines can be greatly benefited from drag reduction technologies.

[1] College of Mechanical and Electrical Engineering, Harbin Engineering University, Harbin 150001, China. E-mail: zhaogang@hrbeu.edu.cn.
[2] College of Mechanical and Electrical Engineering, Harbin Engineering University, Harbin 150001, China.
[3] College of Mechanical and Electrical Engineering, Harbin Engineering University, Harbin 150001, China.
[4] College of Mechanical and Electrical Engineering, Harbin Engineering University, Harbin 150001, China.
[5] College of Mechanical and Electrical Engineering, Harbin Engineering University, Harbin 150001, China.
[6] College of Mechanical and Electrical Engineering, Harbin Engineering University, Harbin 150001, China.
*Received 20 May 2010; accepted on July 28 2010

Existing drag reduction methods include micro-bubble (Takahashi et al., 2001), riblets (Lee S J & Lee S H, 2001; LIU et al., 2009), traveling wave surface (PAN et al., 2006), flexible surface(Pavlov, 2006) and surfactant injection (Itoh et al., 2005; Kurokawa & Itou, 2001; LI et al., 2006). Some of the methods have close relations with bionics of which the target is to imitate the biological feature and build the engineering system with some biological functions (LU, 2004; Ball, 2001). The drag reduction methods like riblets and flexible surface mentioned above are all based on bionic features: the shark and dolphin skins respectively. The bionic drag reduction methods take advantage of biological features and have better drag reduction prospect compared with other drag reduction methods.

Shark has a pair of wide gills near its head as shown in Fig.1. When shark is swimming, water jetting out from its gills and forming jetting flow which has important influence on the flow field and the swimming resistance. In order to find out the relations between different jetting directions and the drag reduction effect, a bionic jetting model imitating the shark gill's jetting flow feature is established based on the principles of bionics after which the drag reduction effect and the reasons of drag reduction are simulated and analyzed under different jetting direction conditions.

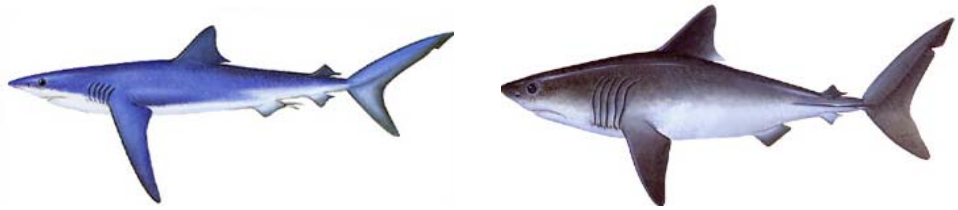

Fig.1: Feature of shark gills

2. BIONIC MODEL

A bionic jetting model is established by arranging round outlets on a flat plate as shown in Fig.2. Like shark gills, water can jet from the round outlets and form the jetting flow. In order to obtain the drag reduction effects under different jetting directions, only a piece of plate with one outlet is separated from the model which is considered as a model cell. Using this model cell to study jetting flow's drag reduction effect can reduce the complexity observably compared to study the whole model. Parameters of the model cell are as follows: width d = 10 mm, thickness h = 5 mm, diameter Φ = 4mm. The angle of jetting direction θ is defined as shown in Fig.3.

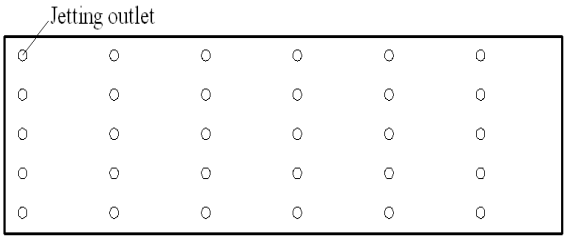

Fig. 2: Bionic jetting model

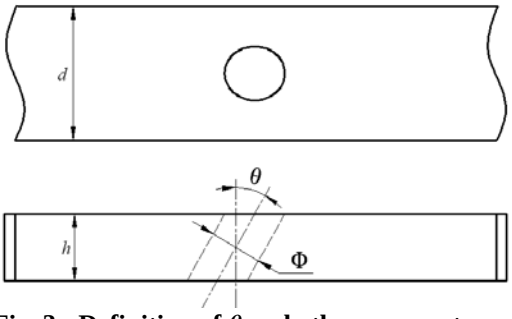

Fig. 3: Definition of θ and other parameters

3. NUMERICAL APPROACH

3.1 Governing equations

The general governing equation in flow field solution is as follows:

$$\frac{\partial(\rho\phi)}{\partial t} + \mathrm{div}(\rho u\phi) = \mathrm{div}(\Gamma_\phi \mathrm{grad}\phi) + S_\phi \tag{1}$$

where ϕ is the dependent variables, S_ϕ the generalized source term, u the velocity vector, Γ_ϕ the diffusion coefficient, ρ the fluid density, t the time. The general governing equation can express equations for continuous, momentum and energy. Parameters in different equations are listed in Table 1, where μ is the coefficient of dynamic viscosity, u_i the velocity components.

Table 1: Parameters in different governing equations

Equation type	$\Gamma\phi$	ϕ	$S\phi$
Continuous	0	1	0
Momentum	μ	u_i	$-\partial p / \partial x + S_i$
Energy	k/c	T	S_T

3.2 Turbulence model

SST (shear stress transport) turbulence model has high accuracy and better algorithm stability in boundary layer simulation and also gives a highly accurate predictions of the onset and the amount of flow separation(LU, 2004; Ball, 2001). For this reason, using SST turbulence model to research drag reduction characteristics near the wall can obtain accurate simulation result. The turbulent momentum and turbulent frequency equations of SST are as follows (Menter, 1994; ZHANG et al., 2009):

$$\frac{d(\rho k)}{dt} = \tau_{ij}\frac{\partial u_i}{\partial x_j} - \beta^* \rho\omega k + \frac{\partial}{\partial x_j}\left[(\mu + \sigma_k \mu_t)\frac{\partial k}{\partial x_j}\right] \tag{2}$$

$$\frac{d(\rho\omega)}{dt} = \tau_{ij}\frac{\partial u_i}{\partial x_j}\frac{\gamma\rho}{\mu_t} - \beta\rho\omega^2 + \frac{\partial}{\partial x_j}\left[(\mu + \sigma_\omega \mu_t)\frac{\partial \omega}{\partial x_j}\right] + 2\rho(1-F_1)\sigma_{\omega 2}\frac{1}{\omega}\frac{\partial k}{\partial x_j}\frac{\partial \omega}{\partial x_j} \tag{3}$$

3.3 Computational domain and boundary conditions

Under different jetting velocity conditions, preliminary simulations indicates that the flow field is stable when the distance from the wall exceeds 2mm according which the height of computational domain fixed on 6mm could be adequate for drag reduction research. On the other hand, since the jetting outlet has little influence on the upstream flow field, we can place the outlet near the upstream of the computational domain. Based on the bionic jetting model cell, a jetting flow computational domain is established with dimensions of X:Y:Z = 50mm:10mm:6mm as shown in Fig.4. For comparison a contrast computational domain without jetting outlet is also given in Fig.5.

In this work, a fully developed turbulent boundary layer must be acquired for better studying the drag reduction effects under different jetting direction conditions, so some special treatments on computational domain are taken as follows: a longer computational domain used to acquire fully developed turbulent boundary layer is established as shown in Fig.6. This computational domain has dimension X∶Y∶Z = 100mm∶10mm∶6mm. In this computational domain, boundary conditions are as follows: mean velocity of inlet is 20 m/s, turbulence intensity is 5% and the outlet pressure is zero. The velocity, turbulent kinetic energy and turbulence dissipation at the outlet of this computational domain which would be used as the inlet boundary conditions of the jetting flow computational domain can be obtained by numerical calculation as shown in Fig.7. After above settings a fully developed turbulent boundary layer is obtained in the whole jetting flow computational domain. Such special treatments can reduce the length of the jetting flow computational domain and make the computing resources being utilized effectively.

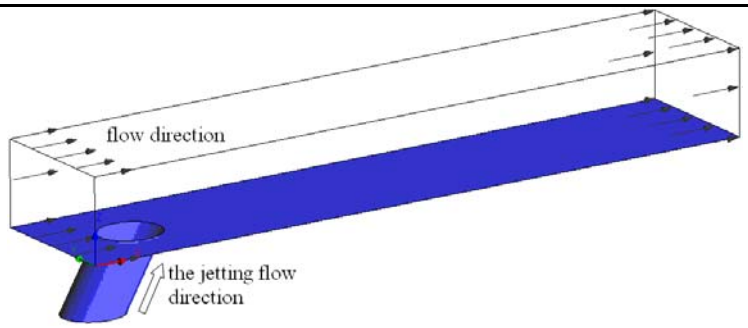

Fig. 4: Jetting flow computational domain

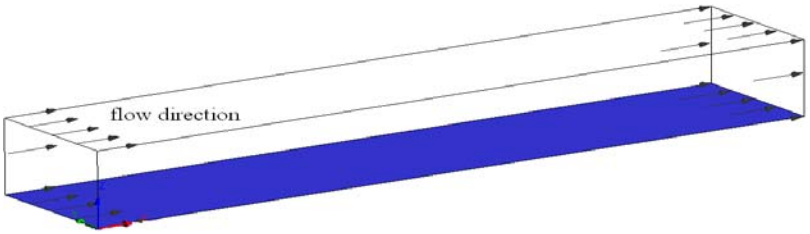

Fig. 5: Contrast computational domain

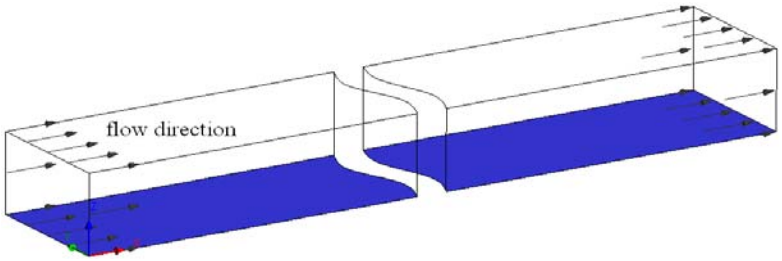

Fig. 6: The longer computational domain

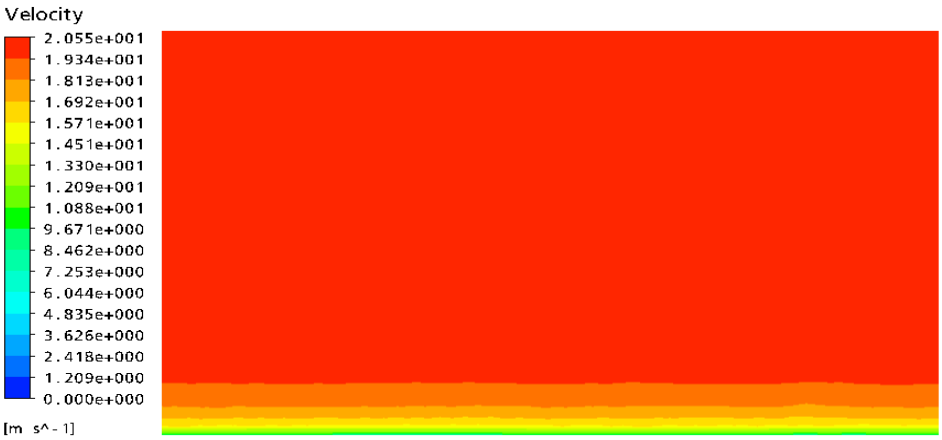

a) Inlet velocity condition of the jetting flow computational domain

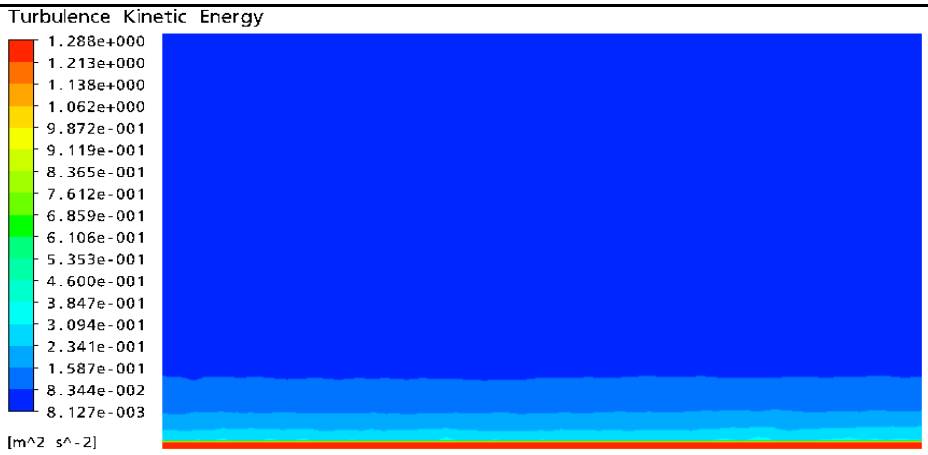

b) Inlet turbulent kinetic energy of the jetting flow computational domain

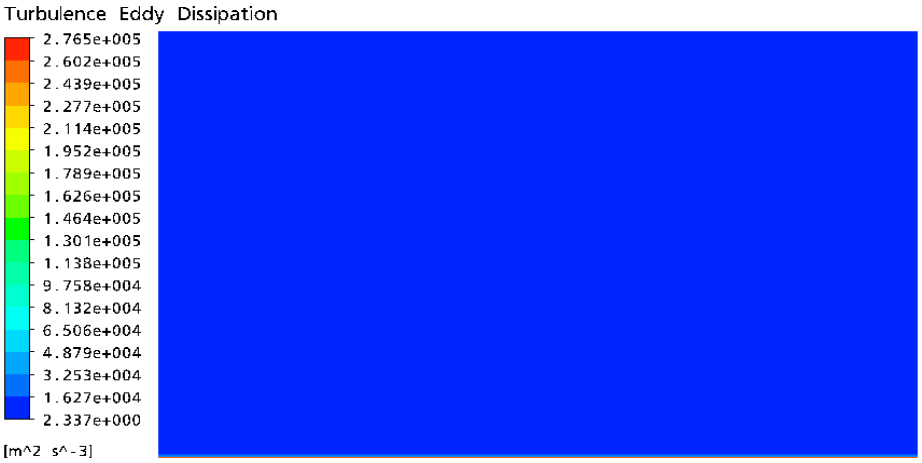

c) Inlet turbulence dissipation of the jetting flow computational domain

Fig. 7: Inlet conditions of the jetting flow computational domain

3.4 Meshing

Because of the influence of the jetting outlet, regular hexahedron grid is not easy to acquire, so a tetrahedron grid is carried out as shown in Fig.8(a). Inflated mesh is used in near-wall regions to improve accuracy in turbulent boundary layer simulation as shown in Fig.8(b), the none-dimension distance y^+ was about 1.

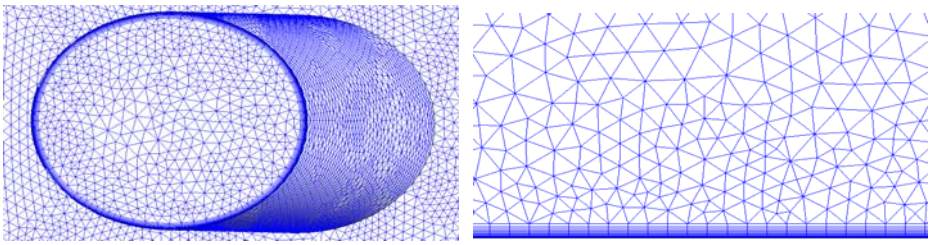

a) Meshing of the jetting inlet　　b) Inflated mesh near the wall

Fig. 8: The computational mesh

3.5 Drag reduction effect evaluation

Drag reduction effect is evaluated by comparing the total drag resistance of the bionic jetting model with the contrasted flat plate model. Drag reduction rate is defined as follows:

$$\eta = \frac{F_D - F_S}{F_D} \times 100\% \tag{4}$$

where F_S is the total drag resistance of the bionic jetting model, F_D the total drag resistance of the contrasted flat plate model. The total drag resistance is

$$F = f + f^* \tag{5}$$

where f is the total viscous resistance, f^* the total pressure drag.

4. RESULTS AND DISCUSSIONS

Since viscous resistance and pressure drag have close relations with the wall shear stress and the static pressure, the wall shear stress and the static pressure are studied in detail when jetting velocity v equals 1.0m/s.

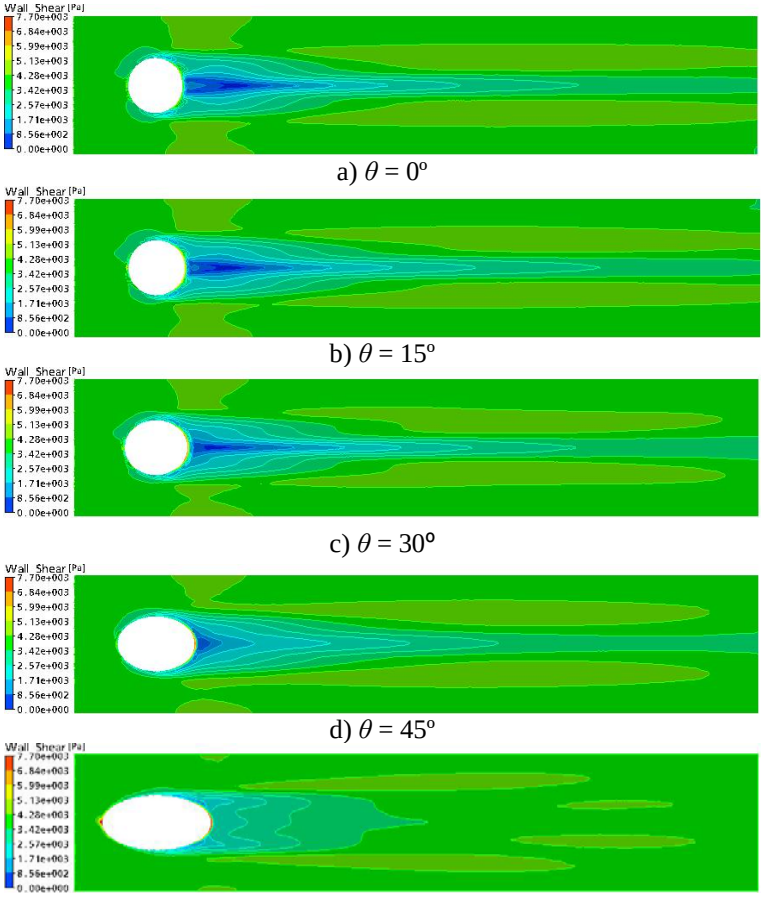

a) θ = 0º

b) θ = 15º

c) θ = 30º

d) θ = 45º

e) θ = 60º

Fig. 9: Comparison of the wall shear stress under different jetting directions (v=1m/s)

The wall shear stress distributions (v=1.0m/s) of bionic jetting model under different jetting directions are shown in Fig.9. It can be seen that there is a shear stress decreased region (the blue region) at jetting outlet's downstream when θ = 0º, 15º, 30º, 45º and 60º. At both sides of the shear stress decreased region, there are two shear stress increased regions (the yellow regions). This phenomenon indicates that the jetting flow has changed the distribution of wall shear stress. Areas of these two kinds of regions are affected by different jetting directions and behave in different viscous resistance. When the area of shear stress decreased region is larger than the shear stress increased region, bionic jetting model's viscous resistance will be reduced.

The static pressure of the flow field (section location y=5mm, v=1.0m/s) under different jetting direction conditions are shown in Fig.10. Obviously, there exists a static pressure decreased region (the green region) at jetting outlet's downstream when θ = 0º, 15º, 30º, 45º and 60º. This region has influence on static pressure distribution near the jetting outlet and makes the pressure drag on the outlet be reduced. When θ increases from 0º to 60º, the area of this green region would be decreased and result in the pressure drag decrease.

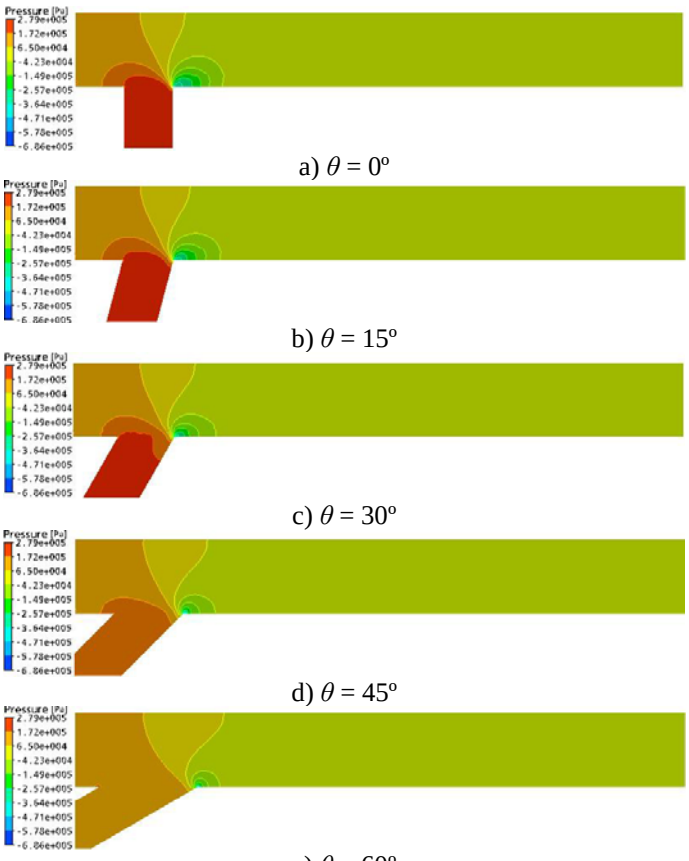

a) θ = 0º

b) θ = 15º

c) θ = 30º

d) θ = 45º

e) θ = 60º

Fig. 10: Comparison of the static pressure under different jetting directions (v=1m/s)

Numerical simulation results of viscous resistance, pressure drag and drag reduction rate under different jetting direction conditions are shown in Fig.11, Fig.12 and Fig.13. In order to find out the best jetting direction condition, the mean drag reduction effect under different jetting direction conditions must be evaluated. The mean viscous resistance $\overline{f}$, mean pressure drag $\overline{f*}$, mean viscous resistance variation $\overline{\Delta f}$ and mean pressure drag variation $\overline{\Delta f*}$ are given in Table 2. It can be seen from Fig.10 that viscous resistance is affected by jetting directions under a certain jetting velocity condition, mean viscous resistance in Table 2 indicates that θ=15º is better for drag reduction. It can be seen from Fig.11 and Fig.12

that the minimum pressure drag and the maximum drag reduction rate are all obtained when θ =30º under a certain jetting velocity condition; a higher jetting velocity condition will help to reduce the pressure drag and acquire better drag reduction effect.

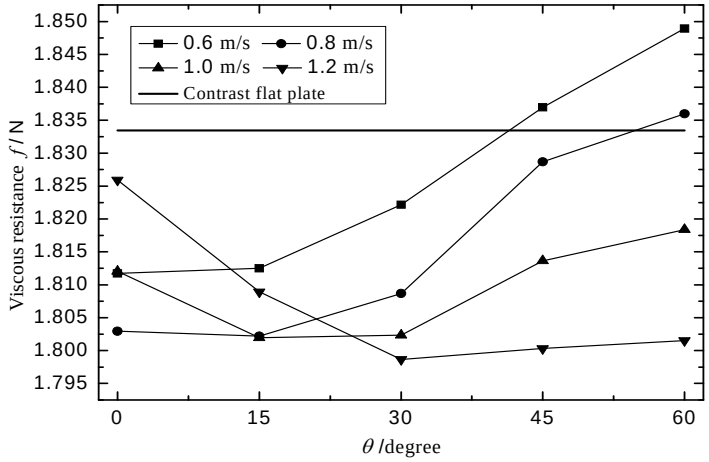

Fig. 11: Viscous resistances under different jetting direction conditions

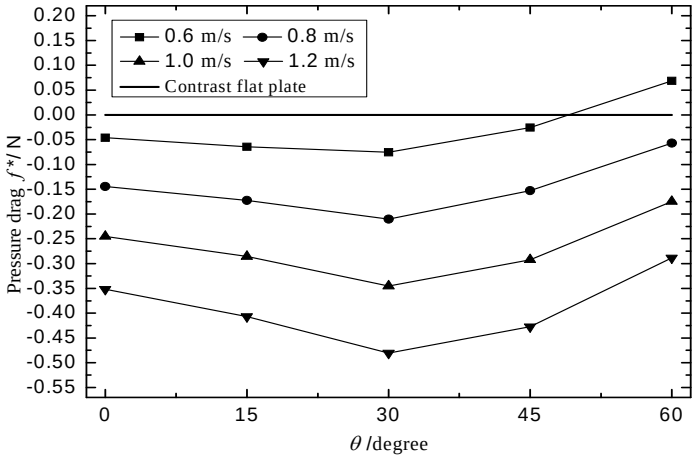

Fig. 12: Pressure drag under different jetting direction conditions

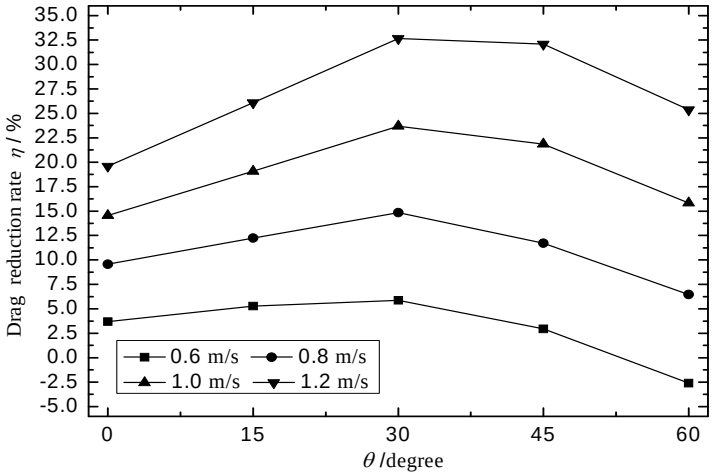

Fig. 13: Drag reduction rate under different jetting direction conditions

In Table 2, $\overline{\Delta f^*}$ is nearly an order of magnitude higher than $\overline{\Delta f}$ under a certain jetting direction condition which indicates that although all the viscous resistance and pressure drag contribute to drag reduction, the main reason of drag reduction is the decreased pressure drag being affected by different jetting directions.

Table 2: Average and average variation of viscous resistance and pressure drag

		$\overline{f}$ (N)	$\overline{f^*}$ (N)	$\overline{\Delta f}$ (N)	$\overline{\Delta f^*}$ (N)
Contrast plate		1.83344	0	——	——
Bionic jetting plate	θ= 0º	1.81316	-0.19685	0.02028	0.19685
	θ=15º	1.80639	-0.23227	0.02705	0.23227
	θ=30º	1.80796	-0.27779	0.02548	0.27779
	θ=45º	1.81990	-0.22452	0.01354	0.22452
	θ=60º	1.82621	-0.11294	0.00723	0.11294

5. CONCLUSION

Based on the bionic jetting model, influence of different jetting directions on drag reduction effect are investigated when flow field velocity is 20m/s. Numerical simulation shows that :

1. The jetting flow under different direction conditions can affect the distribution of wall shear stress and static pressure which results in the variation of the model's viscous resistances and pressure drag;

2. Under certain jetting velocity condition, maximum drag reduction rate can be obtained when θ = 30º which means θ = 30º is the best jetting direction for drag reduction;

3. Analysis of the mean viscous resistance and the mean pressure drag indicates that $\overline{\Delta f^*}$ is nearly an order of magnitude higher than $\overline{\Delta f}$, so the main reason of drag reduction is the decreased pressure drag which is affected by different jetting directions.

REFERENCES

Ball P. (2001). Life's lessons in design. *Nature, 409*: 413.

Itoh M,Tamano S, Yokota K, et al. (2005). Velocity measurement in turbulent boundary layer of drag-reducing surfactant solution. P*hysics of Fluids.075107,17.*

Kurokawa Y, Itou M. (2001). Visualization of turbulent structure in the drag-reducing flow of aqueous surfactant solution. *Proceedings of the 14th Australasian FluidMechanics Conference.877*.

Lee S J, Lee S H. (2001). Flow field analysis of a turbulent boundary layer over a riblet surface.*Experiments in Fluids.30,*153.

LIU Z Y, HU H B, SONG B X, et al. (2009). Numerical simulation research about riblet surface with different spacing. *Journal of System Simulation.21,*6025.

LI F C, Kawaguchi Y, Hishida K, et al. (2006). Investigation of turbulence structures in a drag-reduced turbulent channel flow with surfactant additive by stereoscopic particle image velocimetry. *Experiments in Fluids*, *40*, 218.

LU Y X. (2004). Significance and progress of bionics. *Bionics Engineering.1*,1.

Menter F R. (1994). Two-equation eddy-viscosity models for engineering applications. *AIAA Journal, 32*, 1598.

PAN G, GUO X J,HU H B. (2006). Numerical simulation of semicircular traveling wave surface and study on its drag-reduction mechanism. *Journal of System Simulation*, *18*: 3073.

Pavlov V V. (2006). Dolphin skin as s natural anisotropic compliant wall. *Bioinspiration and Biomimetics*, *1*,31.

Takahashi T, Kakugawa A, Kodama Y, et al. (2001). Experimental study on drag reduction by microbubbles using a 50m-long flat plate ship. Second International Symposium on Turbulence and Shear Flow Phenomena. *Stockholm ,Sweden.1,*175.

ZHANG C C, REN L Q, WANG J, et al. (2009). Simulation on flow control for drag reduction of revolution body using bionic dimpled surface. *Acata Armamentarii. 30*,1066.